Two Coordination Polymers Synthesized from Various *N*-Donor Clusters Spaced by Terephthalic Acid for Efficient Photocatalytic Degradation of Ibuprofen in Water under Solar and Artificial Irradiation

Amina Adala,* Nadra Debbache, and Tahar Sehili

Cite This: *ACS Omega* 2022, 7, 9276−9290

Read Online

ACCESS | Metrics & More | Article Recommendations | SI Supporting Information

ABSTRACT: Two coordination polymers CP1 $\{[Zn(II)(BIPY)-(Pht)]_n\}$ and CP2 $\{[Zn(HYD)(Pht)]_n\}$ (BIPY = 4,4′-bipyridine, Pht = terephthalic acid, and HYD = 8-hydroxyquinoline) have been successfully synthesized by a hydrothermal process using zinc aqueous solution. The so-prepared compounds were characterized by X-ray diffraction (XRD), Fourier transform infrared (FTIR) spectroscopy, UV−visible spectroscopy, thermogravimetric analysis (TGA), and cyclic voltammetry. XRD pointed to a crystalline phase for CP1, while CP2 required recrystallization, FTIR spectroscopy established the presence of characteristic bands for all the ligands, and TGA showed thermal stability up to 100 °C. The electrochemical study showed a good charge transfer between the ligands and Zn metal for both materials. The UV−vis spectra displayed a strong absorption band spreading over a wide wavelength range, encompassing UV and visible light, with a band gap of 2.69 eV for CP1 and 2.56 eV for CP2, both of which are smaller than that of ZnO. This provides an advantageous alternative to using ZnO. The 5×10^{-5} mol L^{-1} ibuprofen decomposition kinetics under solar and UV light were studied under different irradiation conditions. Good photocatalytic properties were observed due to their high surface area.
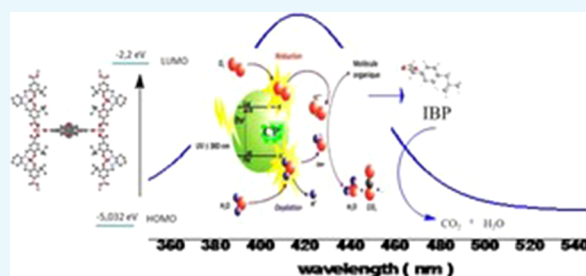
1. INTRODUCTION

Ibuprofen (2-(4-isobutylphenyl)propanoic) (IBP) is the first of the nonsteroidal anti-inflammatory drugs derived from propionic acid to be marketed in most countries. It is mainly used to relieve the symptoms of arthritis, primary dysmenorrheal, and pyrexia and used as an analgesic, especially in the case of inflammation. This drug is used worldwide; several studies have proven its presence in wastewater treatment plant effluents and natural waters. Hence, we chose it as a model substance in our work (Scheme 1).[1−5]

Scheme 1. IBP Structure
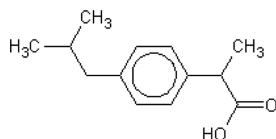
Thousands of tonnes of IBP are consumed worldwide each year, and this amount reflects the amount that will eventually end up in the environment.[6] Much research has been done to assess the conditions under which IBP and its products can be withdrawn. Ibuprofen has been subjected to different treatments: biological methods are not suitable to treat a certain number of drugs properly due to the short residence time in

activated sludge tanks, nonbiodegradability, or toxicity to bacteria.[7] It will surely be desirable to develop treatment methods adapted to this problem in the coming years. Some authors report good results from various advanced oxidation (TOA) techniques: ozonation, UV/H$_2$O$_2$, or O$_3$/H$_2$O$_2$.[8]

The objective of this study is to propose a new technique of organic matter degradation (IBP), which is solar photocatalysis, using the sun as a renewable energy source and within the framework of sustainable development. UV-irradiated metal−organic frameworks (MOFs) (CPs), used as a support for the heterogeneous photocatalytic oxidation process, can be a promising technology for the mineralization of many environmental pollutants. Supported by the abundance of nodes containing metals and organic bonds and thanks to the controllability of synthesis, it is easy to build CPs with an adaptable capacity to absorb light, initiating photocatalytic reactions for specific applications in the degradation of organic pollutants.[9] Among the key factors
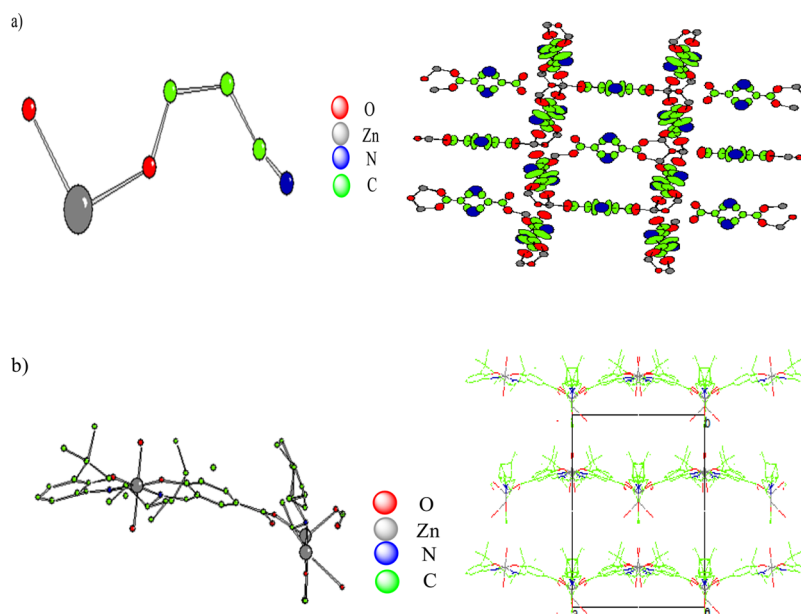
Figure 1. (a) Asymmetric unit and stick model showing the pcu framework structure of CP1. (b) Asymmetric unit and stick model showing the pcu framework structure of CP2.

that affect the effectiveness of the photocatalytic procedure are the optical ban strip (E_g) and sorption O_2/OH^- on semiconductors. These two factors are closely associated with the construction of these materials. The intake−release of O_2/OH^- in water also affects the course of the photocatalytic phenomenon.[10]

The study of phototransformation of ibuprofen in aqueous solutions attracted the attention of several researchers, and Byung-Moon Jun et al. used an organometallic structure (MOF) as an adsorbent to remove selected PhAC (i.e., carbamazepine and ibuprofen (IBP)).[11] In a study by Ning Liu et al., metal-−organic structure (MOF) phases based on iron MIL-88B (Fe) with different facet contents were prepared and used both as photocatalysts and catalysts for the activation of persulfates to eliminate ibuprofen (IBP).[12] Siyu Sun et al. (2021) investigated the degradation of carbamazepine and ibuprofen by photo-Fenton by an iron-based metallo-organic structure in alkaline conditions.[13] To have an environmental approach, our study consists in the study of the photo-degradation of ibuprofen in the natural pH using hydrogen peroxide and other environmental conditions in aqueous environments under UV and solar irradiation.

2. RESULTS AND DISCUSSION

2.1. Crystal Structure. As is known, the construction of CPs depends on several factors, such as the versatility of metal coordination, nature of the organic ligands, and various experimental conditions. In this study, we employed flexible and semirigid bipyridine and 8-hydroxyquinoline ligands and dicarboxylate coligands for synthesizing two CPs because they can provide both structural coordination sites and necessary charge equalization.[14,15] Zn(II) ions are the most commonly reported metal and show excellent luminescence sensing properties when coordinated by multidentate ligands.[16] On the other hand, a current emerging application of CPs is photocatalysis, and some CPs have been proved to be efficient photocatalysts in the degradation of organic pollutants.[17] This

suggests that some Zn(II)-based complexes may possess photocatalytic activities.[18,19]

CP **1** form into crystals in the *Fm-3m* space group and asymmetric unit comprises one Zn(II) and a half of the carboxylic acid with one atom N of the condensed second ligand bipyridine. Refining study indicates that the oxygen atom disordered over multi atoms (Zn(13), C(15), and N(6)) toward tenure constituents two carboxylic ions through the oxygen atom, which confirms a bidentate fashion through the nitrogen atom. The ligand ions L^{2-} coordinate with Zn(II) to form a 3D-network. Interestingly, the OH group of CO_2H and NH constituted during the reaction of condensation of the second ligand bipyridine form a new ring linked with the carboxylic function and form a new ligand, which under the effect of the solvent and temperature complexes directly with Zn(II). The arrangement of each molecule induces a strong pep staking between two amine rings (1.926 (17) Å) and between two phenyl rings (1.89 (18) Å) as is mentioned in Figure 1a.

Unlike CP1, CP2 materializes in the orthorhombic *I*222 space group with the asymmetric unit enclosing I/2 of a Zn_2O cluster, I/4 of a ZnL(OAc) dicarboxylate ligand, and one $[ZnL(H_2O)_2]$ bridging ligand. Zn_2O comprises two bidentate carboxylate groups and one reducing carboxylate group. These Zn_2O rings are attached through $[ZnL(H2F2]$ linking ligands with monodentate oxygen groups to form a one-dimensional chain (Figure 1b). The Zn-salen centers at the ligands are tuned in an equivalent coaxial mode with a Zn−Zn distance of 8.7 Å (Figure 1b). These connections are more attached by the ZnL(OAc) extrapolation ligands by linked carboxylate groups to build a ladderlike I-D coordination polymer (Figure S2). The neighbor ZnL(OAc) units have a Zn−Zn distance of 17.9 Å. CP **2** has a smaller empty space of 45.1% as calculated by PLATON, fixing 5.9% pyridine groups regular with its smaller pore size than CP1. Although CP2 reunites an often smaller void space as opposed to CP1, they have similar dimensions of open channels. As shown in (Figure S2), CP2 obtains its wider block upfront passage of I.2 > 1.2 nm along the [010] direction
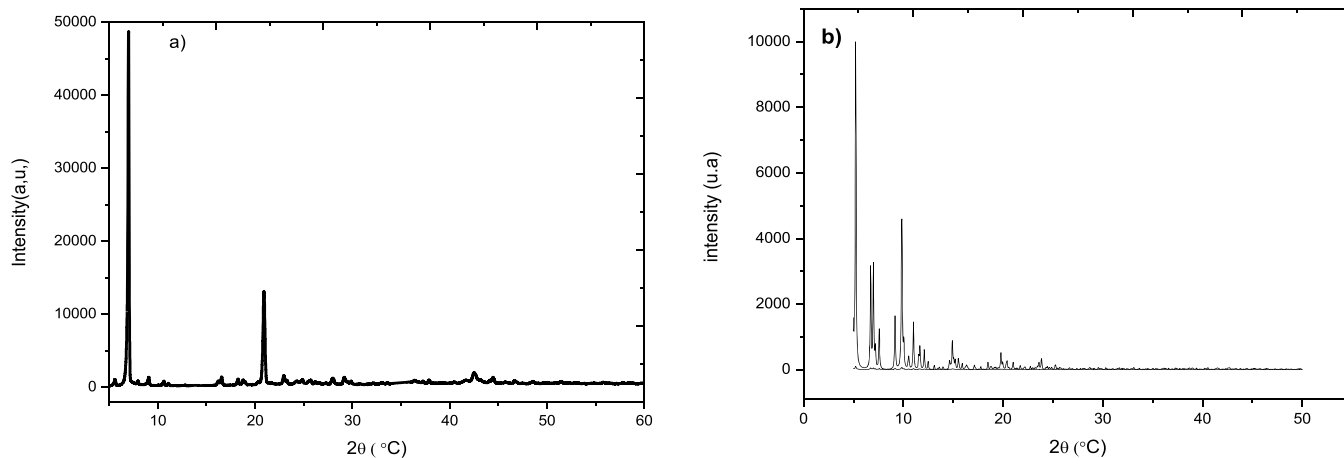
Figure 2. PXRD patterns of the synthesized coordination polymer (a) CP1 and (b) CP2.

in addition to a reduced quadrilateral channel with the diagonal components of I.6 > 0.6 nm along the [100] direction.

2.2. Powder XRD (PXRD) and Thermal Analyses. X-ray diffractograms of the processed synthesized powder are shown in Figure 2a. The peaks observed at the angles 2θ of 6.99°, 31.4°, 9.063°, 10.62°, 11.099°, and 20.90° are attributed to the crystallographic planes (100), (101), (200), (201), (211), and (101) of the cubic structure of the α-CP1 crystal phase. The calculated mesh parameters of the powder are equal to $a = b = c = 25.51930$ Å. The sharpness and intensity of the diffraction peaks indicate good crystallinity of the product. The mean of the crystallite sizes calculated by Scherrer's formula for the most intense peak (100) is of the order of 91.13 nm, and the specific surface of CP1 $\{Zn(II)(BIPY)(Pht)]\cdot H_2O\}_n$ is of the order of 1.13×10^5 m^2 g^{-1}. Bragg R-factor: 98.8, RF-factor: 99.93. The orientations of (101) and (111) in the structure of this polymer showed an outsized specific area of the crystals obtained reported to be beneficial for photocatalytic application due to its good conductivity, which created a fast electron transfer.[20]

Figure 2b shows that the X-ray diffraction patterns of the obtained powders reveal that all the diffraction peaks are assigned to the 2θ peaks of 3.5°, 4.917°, 5.227°, 10.62°, 6.729° and 7.003°, 9.171°, 9.860°, 10.052°, and 11.045°, corresponding to (002), (011), (110), (013), (004), (103), (112), (020), and (211) reflections, agreeing well with the characteristic peaks of $[Zn(II)(HYD)(Pht)]_n$, thus indicating the formation of a structure CP2 less crystalline than CP1 after several recrystallization reactions; the rest of the peaks are in the amorphous form. "Degree of crystallinity (DOC) = 29.85%, amorphous content (wt %) = 70.15%." At the same time, the signal intensity is large, which was probably due to the fact that the organic ligands were fully encapsulated by the MOF shells. The calculated mesh parameters of the powders are equal to $a = 17.92690$ Å, $b = 19.26990$ Å, and $c = 50.45000$ Å. According to the calculations, we find that the specific surface of CP2 is equal to 2.33×10^5 m^2 g^{-1}, which indicates a very large specific surface of these polymers; therefore, these supports CP1 and CP2 contain a large number of accessible pores to be adsorbents or catalysts.

The thermogravimetric analysis (TGA) curves showed that compounds CP1 and CP2 were stable toward oxygen moisture and almost insoluble in common organic solvents, such as CHCl$_3$, MeOH, MeCN, and DMF (Figure 3). To conduct the
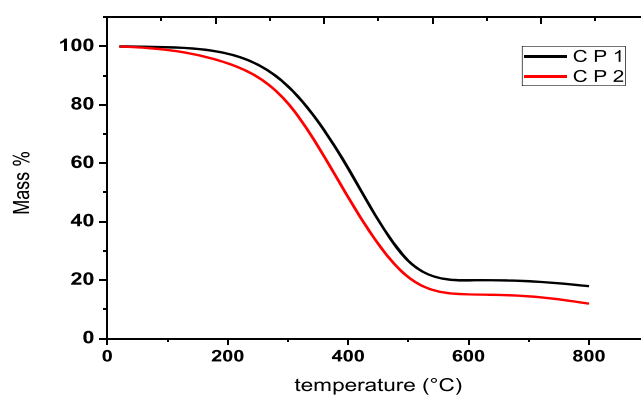

Figure 3. Thermo gravimetric curve (TGA) of the as-synthesized coordination polymers CP1 and CP2.

analysis, CP1 and CP2 were heated in a temperature range of 20 to 800 °C in a nitrogen gas circuit. A mass loss of these materials was observed, starting at 100 °C and up to 500 °C, ascribed to the progressive mineralization of the CPs (observed, 79.83%; calculated, 82%) for CP1 and (observed 85%; calculated, 88%) for CP2. The remaining masses (11.20% for 1 and 30% for 2) are consistent with a ZnO residue. This observation denotes the high thermal stability of the CPs, up to 100 °C, comfortable for the intended use, namely, water treatment, as well as their storage at room temperature, even in the hot season. Above this temperature, a progressive decomposition of the organic component starts. The remaining weights (11.20% for 1 and 30% for 2) are likely consistent with the composition of ZnO.

2.3. FTIR Spectroscopy and Electrochemistry Study. Figure 4 presents the Fourier transform infrared (FTIR) spectra for CP1. The band at 730 cm^{-1} is attributed to the Zn−O group, while the two bands, respectively, at 3014.24 and 3112.71 cm^{-1}, are probably due to water moisture. Compared to the work of "Corinne Allen et al. 2014"[21d] in the region between 3100 and 2450 cm^{-1}, several bands can be assigned to the valence vibration of either aromatic CH or aliphatic CH. The bands that lie at 1504.77 and 1600 cm^{-1} are attributed to the asymmetric valence vibration of O=CO−, while the peak at 1399.76 cm^{-1} is due to the symmetrical valence vibration of O=CO−. The characteristic absorption of the CN group is observed at 1064.33 cm^{-1} due to the condensation of the N atom in the aromatic ring. In the region between 1300 and 700
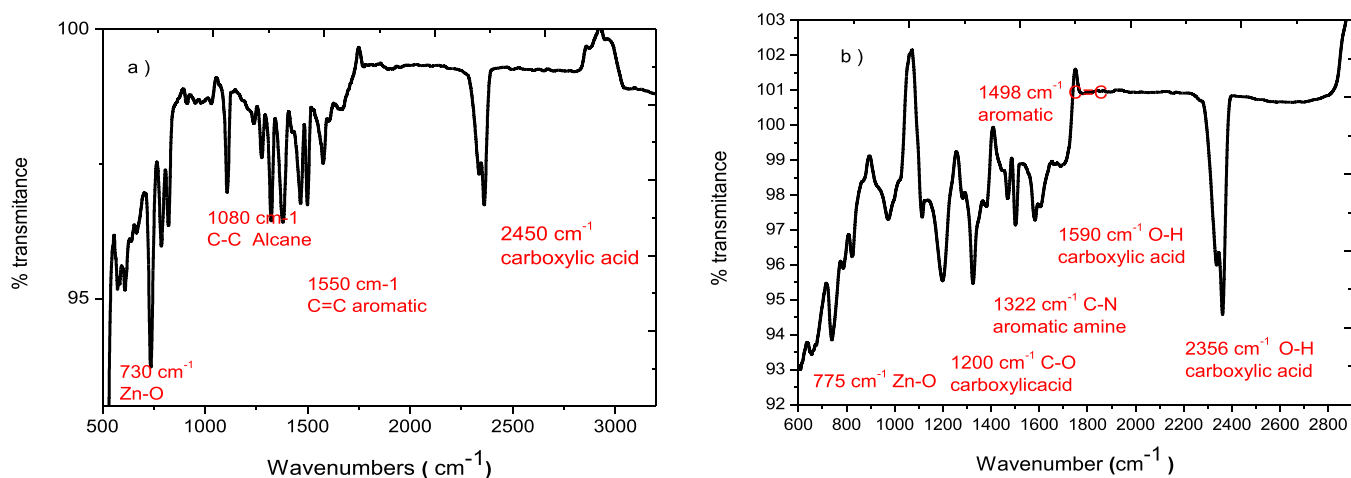
Figure 4. FTIR spectra of the as-synthesized coordination polymers (a) CP1 and (b) CP2.
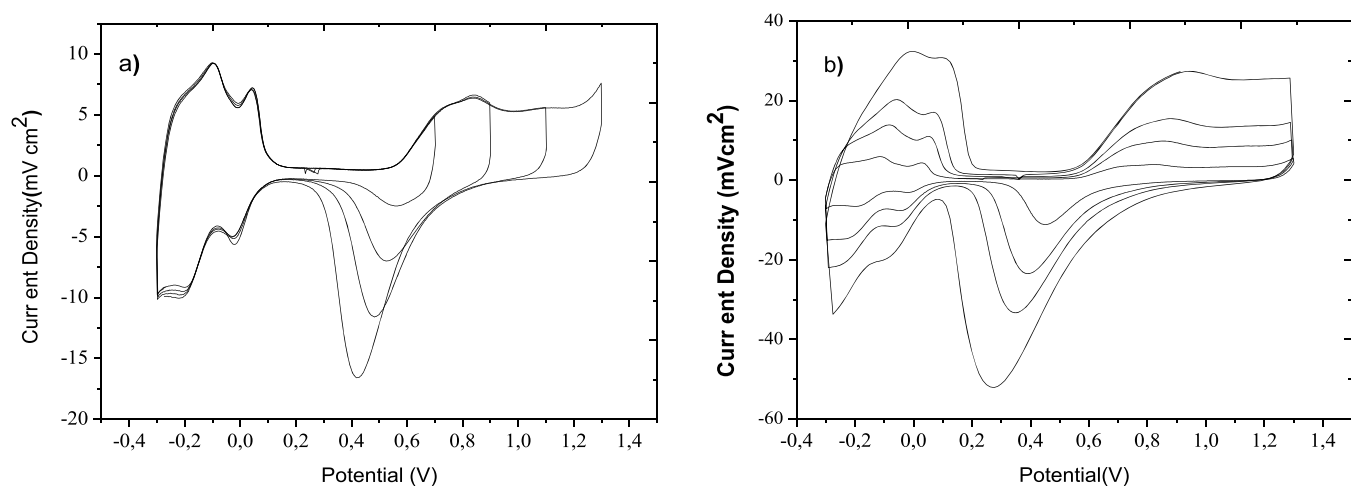

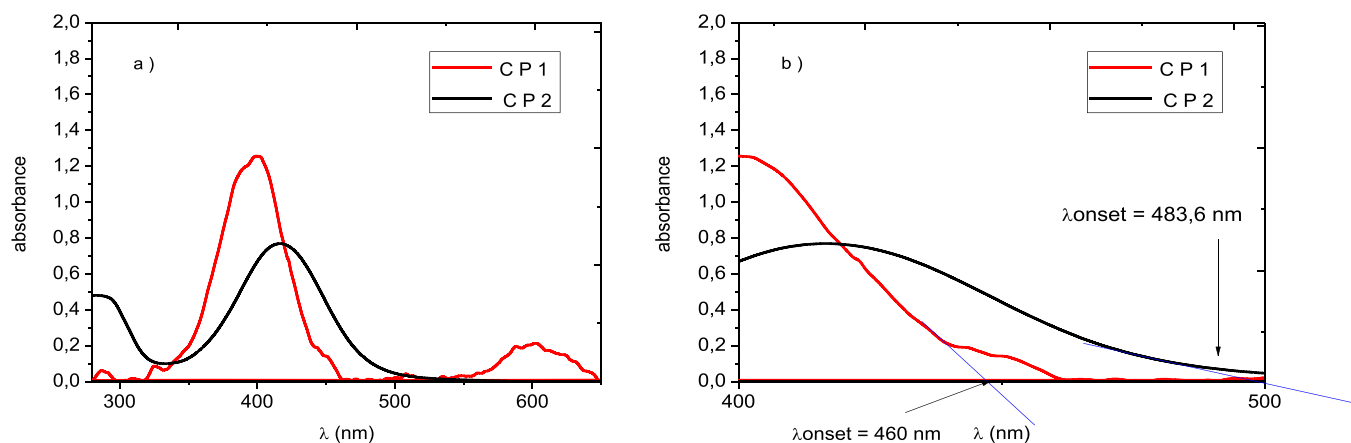**Figure 5.** Electrochemical behavior of the synthesized coordination polymers (a) CP1 and (b) CP2.

Figure 6. (a) UV−visible spectra of CP1 and CP2 powders and (b) determination of the band gaps of the two polymers.

cm^{-1}, several bands are observed, which can be assigned to the vibrations of CH outside the cubic unit cell.

Figure 4b shows the IR spectrum of CP2. As for CP1, the band at 775 cm^{-1} is associated with ZnO. The intense adsorption band at 1394.25 cm^{-1} is due to the symmetrical elongation of the carboxylate group. The bands peaking, respectively, at 1504.33 and 1612.73 cm^{-1} are attributed to the asymmetric valence vibration of O═CO−. The band located

at 1102.84 cm^{-1} corresponds to the CO valence vibration. The CN characteristic absorption band is observed at 1200 cm^{-1} due to the presence of the amine ring. In the 1300 and 700 cm^{-1} region, several bands are observed, which can be assigned to the vibrations of the CH group outside the plane of the structure.
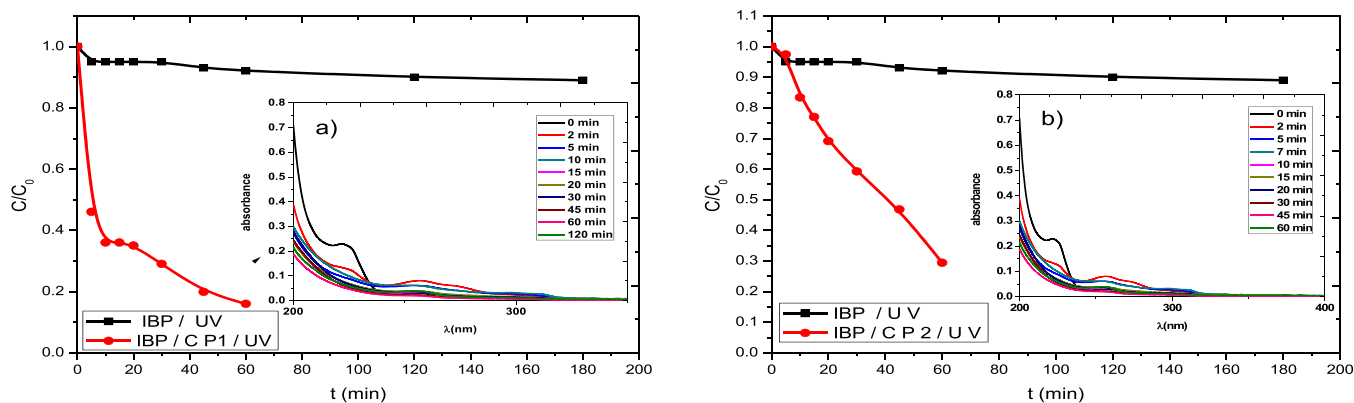
Figure 7. Degradation kinetics of IBP under artificial light irradiation at 365 nm using the synthesized coordination polymers, CP1 and CP2, as catalysts. $[IBP] = 5 \times 10^{-5}$ mol L^{-1}, $[CP1] = [CP2] = 1$ g L^{-1}, pH = 4.5, $T = 293$ K.

These results indicate the couple: the structure of those compounds mostly contains the phthalic acid ligand, which is in good agreement with the XRD results.

Figure 5 exhibits the 10^{-2} mol L^{-1} CP voltammograms. The analyses were carried out in an acetonitrile solution containing 0.1 mol L^{-1} $LiClO_4$, in the presence of 20 mmol L^{-1} $HClO_4$.

A redox couple can clearly be observed in the potential range from +1.4 to −0.3 V for CP1 with two cycles in the reduction scan, the first of which is at 0.2 V and the second is at 0.02 V, and a reversible oxidation peak was recorded at 0.4 V.

The redox couple was observed in the potential range from 1.3 to 0.1 V. One cycle is observed during the sweep of CP2 at 0.8 V and one cycle during the reversible reduction scan at 0.1 V. The mean peak potential $E_{1/2} = (E_{pa} + E_{pc})/2$ is 0.35 V for both CP1 and CP2. This could be attributed to the redox ZnII/ZnI. This oxidative process could be ascribed to an electron transfer from the ligand moieties to Zn or to the ZnO unit.[21] Furthermore, we note the appearance of a new redox system, recorded at a smaller anodic potential than the first cycle for the two polymers. This indicates the formation of an electroactive film on the active surface of the electrode. During the negative scan for the first CP, two new reduction peaks appeared, showing a very good stable reversibility. The preliminary observation of this study showed us that these compounds have the characteristic of an electron-attracting material.

2.4. Photocatalysis. The UV−visible absorption spectra of compounds CP1 and CP2 at 5×10^{-4} mol L^{-1} in DMSO, in the [300; 650] nm spectral region, are shown in Figure 6.

CP1 displays a strong absorption band at 400 nm and a less intense, but still important, band at 600 nm. The two CP2 bands spread from 200 to 500 nm, peaking respectively at 295 and 417 nm. Both absorption bands might be assigned to the $\pi-\pi^*$ transitions within the aromatic rings.

As reported by many authors,[22] the optical gap energy (E_g) of the photocatalyst is one of the most important factors affecting the photocatalytic degradation rate of most pollutants. The E_g values of the two CPs were computed from the measurement of their respective λ onset, using the relationship $E_g = 1240/\lambda$. The latter is derived graphically. It corresponds to the intersection of the straight line extrapolated from the linear portion of the absorption edge with the baseline of the UV spectrum.[23] (Figure 6b). The E_g estimated values are at 2.69 eV for CP1 and 2.56 eV for CP2. These experimentally determined band gap values indicate that the compounds 1 and 2 can show absorption of UV light and therefore have the

potential for the catalytic photodegradation of organic pollutants.

2.4.1. Photodegradation of Ibuprofen in the Presence of Semiconductor CPs. Coordination polymers can be used as photocatalysts in advanced oxidation processes. Their efficiency in the degradation of organic compounds has been reported in the literature.[11−14] The use of these materials is gaining a rising importance owing to the many advantages they offer, particularly their stability, the possibility of their recovery and reuse, their low cost, and their environmental compatibility.

This work focused on understanding the mechanism of the photocatalytic degradation of ibuprofen (IBP), using a coordinating polymer as the heterogeneous photocatalyst. The degradation kinetics of IBP using UV light or sunlight were studied.

The photocatalytic processes CPs/UV and CPs/H_2O_2/UV are used to determine the efficiency of these systems in the degradation of IBP. The influence of some experimental parameters on the rate of degradation such as the initial pH, the concentration of hydrogen peroxide, and the presence of inorganic salts in the solution was evaluated. The intermediate compounds were identified by GC/MS in order to elucidate the degradation mechanisms.

2.4.2. Study of the IBP/CPs/UV System. Figure 7 shows the concentration variations of 5×10^{-5} M IBP as a function of the irradiation time in the presence of 1 g L^{-1} of CP1 and CP2, respectively. The mixture was irradiated with a polychromatic lamp with $\lambda_{max} = 365$ nm. The aim behind choosing this lamp was to minimize the percentage of direct photolysis and work at wavelengths closer to those of the solar spectrum and environmental conditions.

The results indicate that the percentage of IBP abatement at 365 nm by the system UV/CP1 and UV/CP2 is relatively moderate, and the degradation rate was 84% after 60 min of irradiation. The pseudo-first-order reaction rate constant k is 3×10^{-4} min^{-1} ($R^2 = 0.95$) with a half-life of the order of 35.5 min for CP1 and 70.6% for CP2, and the pseudo-first-order reaction rate constant k is 10^{-4} min^{-1} ($R^2 = 0.97$) with a half-life of the order of 69.5 min. The quantity of Zn^{2+} formed during the reaction is negligible (on the order of 10^{-6} M).

We note from these results that the efficiency of the photocatalytic degradation of IBP by catalyst 1 is higher than that by catalyst 2. This may be due to the distinct 3D structure built by the BIPY ligands and pht^{2-} ions in CP1, which either enhances the internal electron transfer, thus creating more
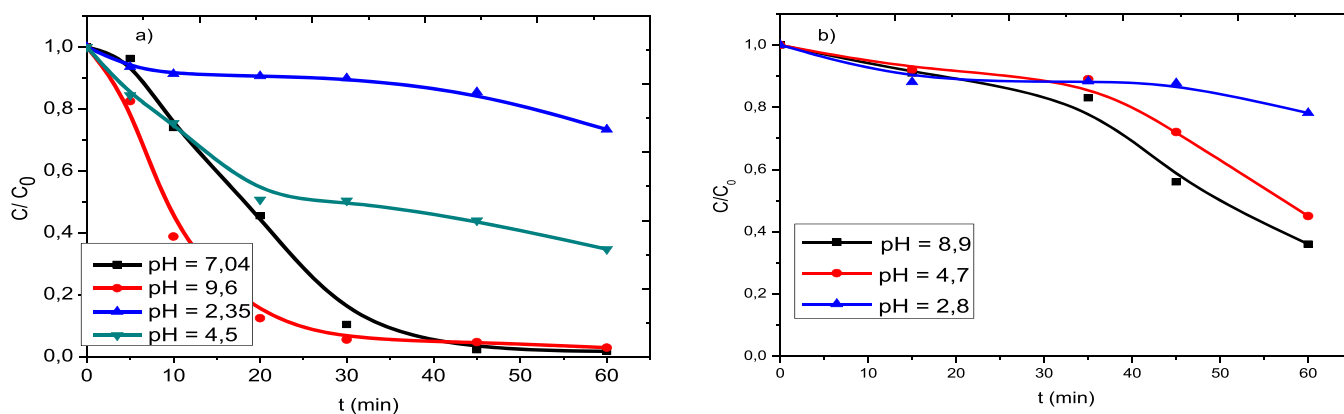
Figure 8. Effect of pH on the degradation rate of IBP under artificial irradiation (365 nm) with the synthesized coordination polymers (a) CP1 and (b) CP2. $[IBP] = 5 \times 10^{-5}$ mol L^{-1}, $[CP1] = [CP2] = 1$ g L^{-1}, $T = 293$ K.
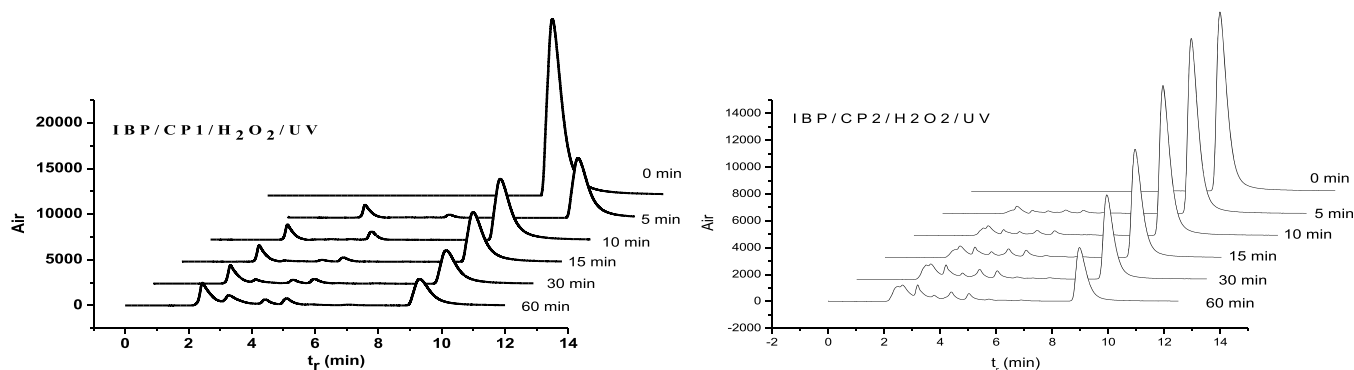

Figure 9. Degradation chromatograms of IBP under artificial light irradiation (365 nm) using the synthesized coordination polymers (CP1 and CP2) as catalysts $[IBP] = 5 \times 10^{-5}$ mol L^{-1}, $[CP1] = [CP2] = 1$ g L^{-1}, $[H_2O_2] = 10^{-3}$ mol L^{-1}, pH = 4.5; $T = 293$ K.

numerous (e$^-$) and holes (h$^+$), or facilitates the sorption of O$_2$/OH$^-$ on the CPs. The specific reasons for the multiple structures need to be further explored. In addition, from the UV−vis semiconductor absorption spectra (Figure 6), we deduced that the photocatalytic activities of these materials could be attributed to the ZnO units formed as already shown in the FTIR spectrum. With UV light, the observed electronic transitions occur between the 2s oxygen orbital and the 4s zinc orbital. With visible UV light, the bands located at 400 and 417 nm result respectively from localized transitions in the amount of energy difference and the half-time. Also, because of the principle of ligand−metal charge transfer, the absorption of light by organic ligands bound by electronic transitions to zinc flowers causes electrons to pass from the rocky bottom state [ML2X2] to the excited state [ML2X2]*. The electrons are then inserted into the conduction band of the oxide having an energy level at the edge of that of the excited state. We have oriented the synthesis to allow the coordination polymers playing the role of double-cap photocatalysts, the ZnO units on one side and the complex principle on the other side, which explains the high efficiency of these two polymers in the field of heterogeneous photocatalysis for the degradation of organic pollutants.[24−27]

2.4.3. Effect of the Initial pH Value. pH is the main factor influencing the ionization state of IBP and the surface of CPs where the photocatalytic process takes place. The effect of solution pH on the photocatalytic degradation of ibuprofen in the presence of CPs was examined. To achieve this, we irradiated an aqueous 5×10^{-5} mol L^{-1} IBP containing 1 g L^{-1}

of CPs at different pH levels. The pH was adjusted with either a few drops of perchloric acid or NaOH.

Figure 8 indicates a higher rate constant in alkaline solutions for both CPs, with k_{app} increasing continuously with increasing pH, within the studied range. The maximal value of the pseudo-first-order rate constant for CP1 was 8.53×10^{-5} M^{-1} s^{-1} ($R^2 = 0.908$), observed at pH = 9.6, and 5.68×10^{-4} M^{-1} s^{-1} ($R^2 = 0.99$), observed at pH = 8.9, for CP2.

As already mentioned in the previous results, probably ZnO is the compound responsible for the degradation of ibuprofen; the possible reason for this behavior is that the presence of vast quantities of OH$^-$ ions on the ZnO surface favors formation of ●OH radicals, which then enhances the photocatalytic degradation of IBP. Conversely, the decrease within the photocatalytic degradation at acidic pH could be due to the dissolution of ZnO at (pH ≤ 3) (Behnajady, Modirshahla, and Hamzavi[18]). This clearly confirms that in the acidic medium, the dissolution of ZnO would occur.

2.4.4. Study of the IBP/CPs/H$_2$O$_2$ System. One way of improving the photocatalytic efficiency of polymers relies on the addition of electron acceptors such as hydrogen peroxide in the reaction medium[28,29] IBP/CPs/H$_2$O$_2$ system. In fact, in the heterogeneous phase, the photocatalytic processes for the degradation of ibuprofen under different conditions are illustrated in Figure 9. The process, with CP (1) and (2) in the presence of H$_2$O$_2$ (with UV), has shown higher activities than direct photolysis in UV and UV/CP systems. The photocatalytic power of CP1 and CP2 in the presence of H$_2$O$_2$ leads to a significant decrease in the concentration of

ibuprofen. A conversion of 97.1 and 77.1% respectively is obtained after 60 min of reaction; the pseudo-first-order reaction rate constant K is 5.47×10^{-2} min^{-1} ($R^2 = 0.955$), with a half-life of approximately 12.67 min, for CP1, and the pseudo-first-order reaction rate constant K is 2.14×10^{-2} min^{-1} ($R^2 = 0.961$), with a half-life of approximately 32.39 for CP2.

Knowing that hydrogen peroxide limits the recombination of charges in semiconductors, for this we varied the concentration of the latter to have the effect of this parameter on the degradation of IBP in the range of 10^{-4} to 10^{-2} mol L^{-1} in the presence of 1 g L^{-1} of the polymers and at natural pH. The results are shown in Figure 10.
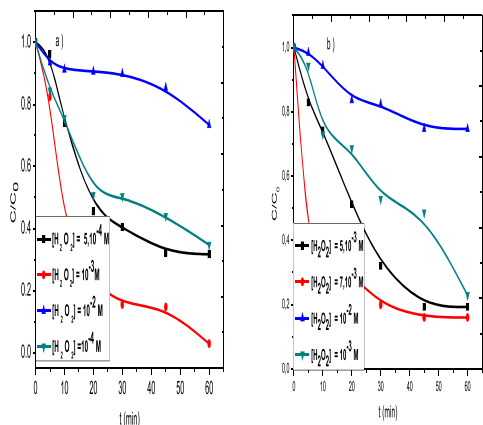

Figure 10. Influence of the initial concentration of H_2O_2 on the photocatalytic degradation kinetics of IBP using the synthesized coordination polymers (a) CP1 and (b) CP2 and artificial irradiation (365 nm). $[IBP]_0 = 5 \times 10^{-5}$ mol L^{-1}, $[CP1] = [CP2] = 1$ g L^{-1}, pH = 4.5, T = 293 K.

The obtained results show that IBP has undergone oxidation in the presence of hydrogen peroxide. The degradation went from 77.1 to 97.1% for CP1 and from 66.53 to 84% for CP2, with the increase in the hydrogen peroxide concentration of 10^{-4} to 10^{-3} mol L^{-1}. This is due to the decomposition of hydrogen peroxide on the surface of CPs to generate hydroxyl radicals. The highest degradation rate of IBP was observed during the first minutes of the reaction, which means that the radical with the highest degradation rate of IBP was observed

during the first minutes of the reaction. This means that the radical species-induced decomposition of hydrogen peroxide takes place with a high speed. The increase in the H_2O_2 concentration would lead to an increase in the hydroxyl radicals generated. This explains the acceleration of the degradation of IBP.

$$CPs + h\nu \rightarrow h_{vb}^+ + e_{bc}^- \tag{1}$$

$$H_2O_2 + h\nu \rightarrow 2^{\bullet}OH \tag{2}$$

$$H_2O_2 + 2e_{bc}^- \rightarrow 2^{\bullet}OH \tag{3}$$

$$H_2O_2 + \acute{e}_{bc} \rightarrow OH^- +^{\bullet} OH \tag{4}$$

$$H_2O_2 + O_2^{\bullet -} \rightarrow O_2 +^- OH + {}^{\bullet}OH \tag{5}$$

In heterogeneous catalysis, the metal is stabilized in the space between the catalyst layers and can efficiently produce hydroxyl radicals from the oxidation of hydrogen peroxide, under free pH conditions and without precipitation of metal under hydroxide form ZnO.

However, increasing the concentration of H_2O_2 above (10^{-2} M) can slow down the degradation process. Excess H_2O_2 could act as a scavenger of HO$^{\bullet}$ radicals, resulting in the generation of HO$_2$ radicals, that is to say less reactive species.

$$H_2O_2 +^{\bullet} OH \rightarrow HO_2 + H_2O \tag{6}$$

$$OH + HO_2^{\bullet} \rightarrow O_2 + H_2O \tag{7}$$
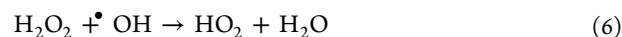
Therefore, the photodegradation described during this work was assumed to follow a similar mechanism to other semiconductors. To confirm this hypothesis, we selected *tert*-butyl alcohol (TBA) as a scavenger of $^{\bullet}$OH radicals. It is documented that TBA is an efficient quenching agent for the $^{\bullet}$OH radical, by capturing the latter via the following reaction.[30−32]

$$^{\bullet}OH + t - BuOH \rightarrow t - BuOH \bullet$$

As it is well known, tertiobutanol is an efficient OH radical scavenger. Hence, no more than 2 mL of t-BuOH was added into a 100 mL solution of IBP/CP1 and IBP/CP2.

The results show that the photodegradation of ibuprofen is considerably slowed, and the degradation rate of IBP is 15.8 and 20.3% for CP1 and CP2, respectively (Figure 11). This confirms that $^{\bullet}$OH is the main species that is responsible for
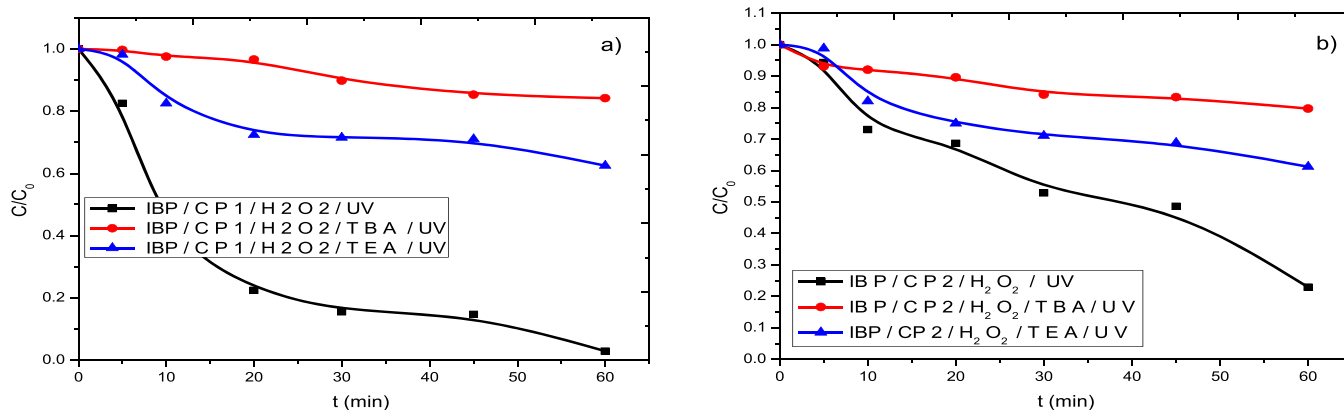

Figure 11. Degradation kinetics of IBP under different conditions, with artificial light irradiation (365 nm), using (a) CP1 and (b) CP2 synthesized coordination polymers as catalysts. $[IBP] = 5 \times 10^{-5}$ mol L^{-1}, $[CP1] = [CP2] = 1$ g L^{-1}, $[H_2O_2] = 10^{-3}$ mol L^{-1}, $[TBA] = [TEA] = 2\%$, pH = 4.5, T = 293 K.

the degradation of the pollutant on the one hand. To determine the probability of existence of some other species liable for the phenomenon of photodegradation, we tried to dam the circulation of the holes by using triethanolamine (TEA) as a scavenger of the holes. From the pace of the kinetics (Figure 11), it can be concluded that the degradation phenomenon for both CP1 and CP2 after the first 30 min is carried out from the holes that are all constant and the adsorption phenomenon is completely unaffected after 30 min.

From the literature and the results obtained, the possible mechanism of photocatalytic photodegradation of pollutants in water using 1−2 complexes as a catalyst can be described as follows (Figure 12):
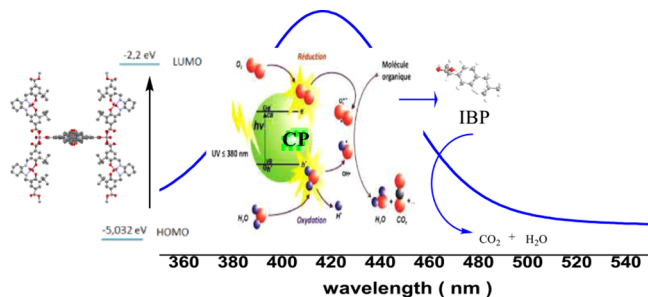

Figure 12. Proposed reaction scheme for the IBP/CPs/H_2O_2 degradation system.

When the CP absorbs photons with energy greater than the value of its forbidden band (HP > E_g = 2.65 eV), an electron passes from the valence band to the conduction band, creating an oxidation site (h^+ hole) and a reduction site (e^- electron). The h^+ holes react with electron donors such as H_2O, OH^- anions, and organic products R adsorbed on the surface of the semiconductor, forming $OH\bullet$ and $R^\bullet$. The e^- reacts with the e^- acceptors such as O_2 to form superoxide radicals $O_2^{\bullet-}$ and subsequently H_2O_2.[33]

2.4.5. IBP Photodegradation in Real Environmental Conditions. To get closer to natural conditions, an important step in our study is monitoring the degradation of IBP under solar irradiation. The experiments were carried outdoors, the solutions being placed at the ground level, in an open space

adjacent to the building hosting our laboratory in Constantine (Figure 17).

Figure 13 shows the degradation kinetics of IBP with the CP1 or CP2/solar UV process where the mixture of IBP, CPs, and H_2O_2 (5 × 10^{-5} mol L^{-1}, 1 g L^{-1}, 10^{-3} mol L^{-1}) has been exposed to natural sunlight. The average intensity of solar radiation measured during the reaction is 0.98 W cm^{-2}. The use of solar irradiation in treatment processes is particularly advantageous because it reduces energy costs, especially in a country like Algeria, where a high solar incidence is abundant and which has been poorly exploited until now.

The results show an acceleration of the reaction rate compared to that obtained under artificial irradiation. The pseudo-first-order rate constant is 1.6 × 10^{-3} M^{-1} s^{-1} (R^2 = 0.98) and 1.05 × 10^{-4} M^{-1} s^{-1} (R^2 = 0.807) with a degradation rate of 99.7 and 97% of CP1 and CP2, respectively, after 60 min (in the inset of Figure 13a,b). The higher rate of degradation under natural irradiation is explained by the existence of photoproducts from irradiations at different wavelengths contained in solar radiation.

To bring these closer to natural environmental conditions, inorganic anions are studied, like chlorides Cl$^-$, bicarbonates HCO_3^-, and carbonates CO_3^{2-}, species that are very present in groundwater, contributing in a significant way to the alkalinity of water.

To study the effect of certain inorganic salts, which are presumably found in natural waters, sodium hydrogen carbonate and common salt are added at different concentrations within the initial solution, and therefore, the rate constants of the corresponding first order were measured.

In our experiments, the pH of the medium was not adjusted. Changes in pH during reaction are shown in Table 1.

Table 1. Variations in pH during Treatment with the CP1/UV System: IBP (5 × 10^{-5} M); CP1 (1 g L^{-1})

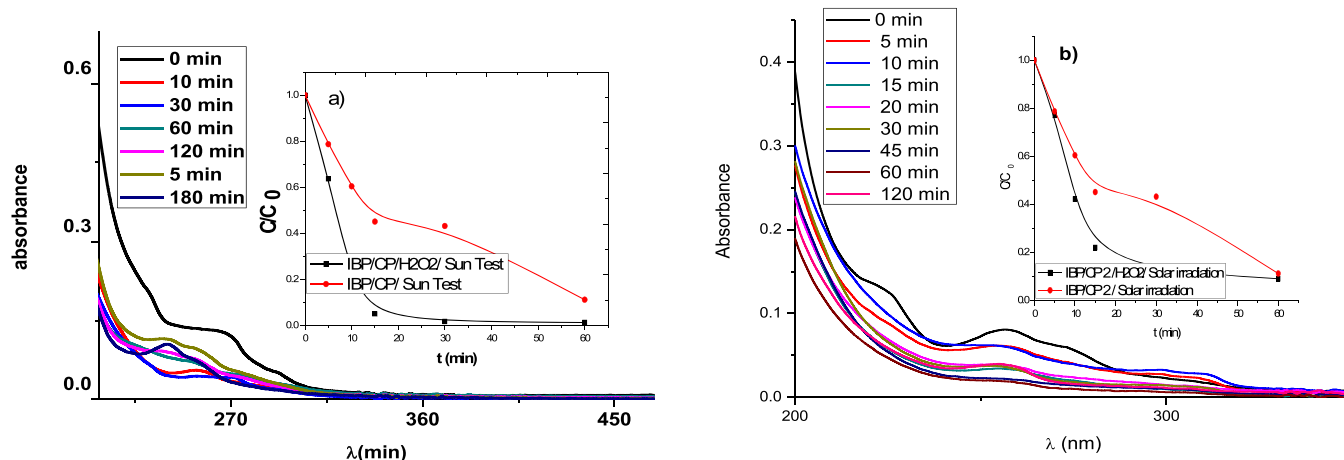|	C (mol L^{-1})	initial pH	final pH
NaCl	0	3	3.1
	10^{-3}	3.5	6.1
	10^{-2}	3.7	6.3
NaHCO$_3$	0	3.0	3.1
	10^{-3}	3.4	6.4
	10^{-2}	3.6	6.5

Figure 13. (a) UV−vis spectrum of degradation of IBP under simulated irradiation using the coordination polymer CP1 and (b) CP2 synthesized used as the catalyst in the presence of H_2O_2. [IBP] = 5 × 10^{-5} mol L^{-1}, [CP] = 1 g L^{-1} [H_2O_2] = 10^{-3} mol L^{-1}.
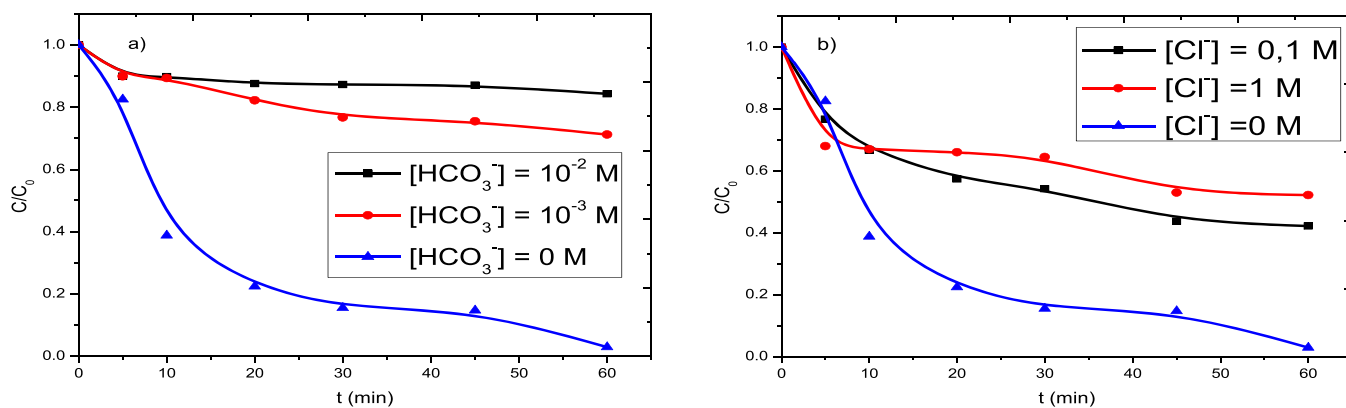
Figure 14. (a) Effect of bicarbonate and (b) chloride ions, on the degradation of ibuprofen by CP1/H$_2$O$_2$. [IBP] = 5 × 10^{-5} M, [CP1] = 1 g L^{-1}, [H$_2$O$_2$] = 10^{-3} mol L^{-1} under solar irradiation.
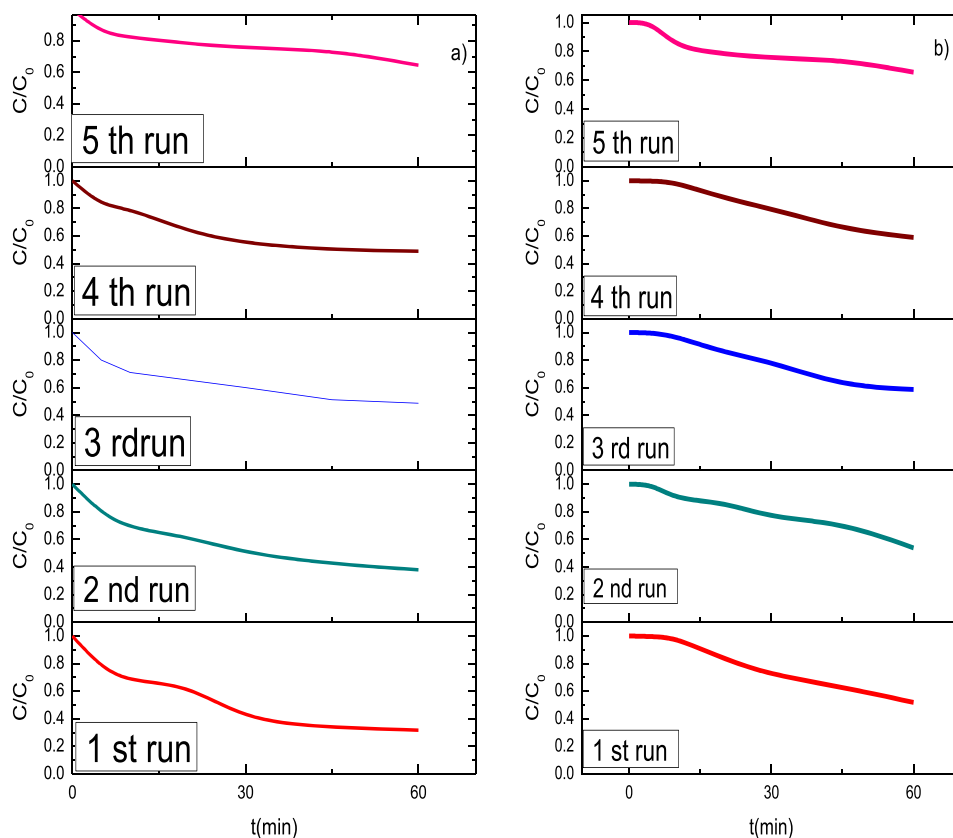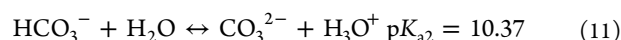

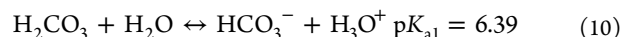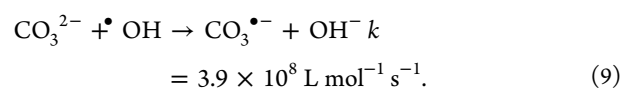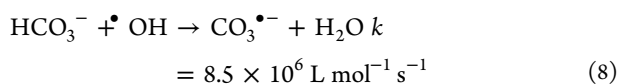**Figure 15.** Stability and reuse of the synthesized coordination polymers (a) CP1 and (b) CP2 after irradiation at 365 nm. [IBP] = 5 × 10^{-5} mol L^{-1}, [CP1] = [CP2] = 1 g L^{-1}, [H$_2$O$_2$] = 10^{-3} mol L^{-1}, T = 293 °C, pH = 4.5.

In natural waters, bicarbonate ions are more present as ions (pK_a HCO$_3^-$/CO$_3^{2-}$ = 10.2), (pH 6.5−8.5) and their concentration rarely exceeds 0.05 mol L^{-1}.[34]

The influence of these ions on the degradation kinetics is shown in Figure 14a. The results show an inhibition in the phototransformation phenomena at a concentration of 10^{-3} mol L^{-1}, inducing a reduction rate of 28.8% after 1 h of solar irradiation. This can be explained by an enhanced competition for the adsorption and by the trapping of OH radicals according to the reaction:[29]

$$HCO_3^- + {}^\bullet OH \rightarrow CO_3^{\bullet-} + H_2O \ k$$
$$= 8.5 \times 10^6 \ \text{L mol}^{-1} \ \text{s}^{-1} \tag{8}$$

$$CO_3^{2-} + {}^\bullet OH \rightarrow CO_3^{\bullet-} + OH^- \ k$$
$$= 3.9 \times 10^8 \ \text{L mol}^{-1} \ \text{s}^{-1}. \tag{9}$$

$$H_2CO_3 + H_2O \leftrightarrow HCO_3^- + H_3O^+ \ pK_{a1} = 6.39 \tag{10}$$

$$HCO_3^- + H_2O \leftrightarrow CO_3^{2-} + H_3O^+ \ pK_{a2} = 10.37 \tag{11}$$

As shown in the literature, a carbonate salt (HCO$_3^-$/CO$_3^{2-}$) possesses an inhibitory effect on the degradation efficiency of organic compounds. The work of Daneshvar et al.[35] shows that the presence of mineral salts (NaCl, NaHCO$_3$, and Na$_2$CO$_3$) decreases the speed of degradation of 4-nitrophenol.[35] Kochany et al.[36] studied the photodegradation of bromoxynil 3,5-dibromo-4-hydroxyphenyl cyanide (λ > 300 nm) in

solution in the presence of carbonate and bicarbonate ions. An inhibitory effect has also been observed.[36]

In the case of chlorides, Figure 14b, the results show a slowing down of IBP disappearance. In our experiments, the final pH was 6.1, lower than CP1's pH (8.6). Many studies have found that chlorides inhibit both adsorption and photodegradation phenomena at neutral pH.[37,38] Daneshvar et al.[35] report that the addition of Cl⁻ ions results in a small decrease in the speed of reduction of 4-nitro phenol.[35] One possible explanation is that chloride anions, like other halides, are known to trap positively charged photogenerated holes.[39] In addition, the ●Cl radicals are very powerful oxidants, as are the ●OH radicals, which cause the competition between these two radicals to catch the electrons during the transfer of the charge of the semiconductor, tearing of a charged or addition/elimination in a positively charged hole,[40−42] which led to the inhibition of the photocatalytic reaction.

2.4.6. Stability and Reuse of CPs. The recyclability of CP1 and CP2 was evaluated with a series of successive degradation experiments of IBP in the CP−H_2O_2 systems. The reuse of the solid was evaluated under identical oxidation conditions. To know the number of times that the support can be used as an adsorbent, the following experiments were carried out. At the end of the oxidation process, the solid is removed from the reactor by filtration and dried in an oven at a moderate temperature (50 °C). The recovered adsorbent was added to a fresh solution of (IBP-H_2O_2) (5×10^{-5} mol L⁻¹; 10^{-3} mol L⁻¹), and the percentage of degradation was recorded after 60 min of reaction (run 2). Then, the adsorbent, which was used in the previous run (run 2), was separated and added to a fresh solution of ibuprofen, the percentage of degradation was recorded (run 3), and so forth.

The results presented in Figure 15 showed that the solid could be reused for five cycles, and the percentage of degradation of IBP was estimated for the five successive cycles at 68.3, 62, 51.2, 51, and 36% for CP1 and 48.2, 46.2, 41.2, 41, and 34.5% for CP2. It is essential to note that for the last test, the quantity of the solid has greatly decreased for both photocatalysts, hence the decrease in their effectiveness.

From these results, it can be seen that the reused catalysts retained a catalytic activity almost as effective as the fresh material, and it is therefore concluded that the support could be effectively recycled.

2.5. Mineralization Study. Mineralization indicates that the pollutant is completely transformed into mineral carbon. We followed the mineralization of IBP through chemical oxygen demand (COD) measurements of the IBP−CPs−H_2O_2 mixture (5×10^{-5} mol L⁻¹; 1 g L⁻¹; 10^{-3} mol L⁻¹) under artificial irradiation, as a function of the time, for 12 h.

We have chosen to work at free pH, which is acidic. It is important to note that the COD decreases more slowly regardless of the CPs, Figure16.

The COD reduction percentages under artificial irradiation for CP1 and CP2 are successively 92 and 77% after 12 h. Such a poor removal efficiency is attributed to the formation of transformation photoproducts that are more refractory to degradation than the CPs/IBP/H_2O_2 mixture, thus needing more time to be mineralized.

2.6. Identification of Byproducts and the Degradation Mechanism. The mechanism of the photodegradation of organic pollutants catalyzed by semiconductive materials was reported by Chen and Paola.[40−48] The band gaps (2.69 eV) of
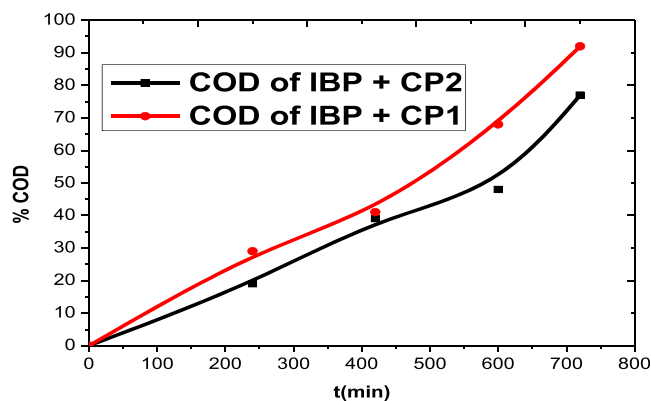

Figure 16. Abatement of COD during irradiation of the mixture ([IBP] = 5×10^{-5} mol L⁻¹, [CP1] = [CP2] = 1 g L⁻¹, [H_2O_2] = 10^{-3} mol L⁻¹, pH = 4.3 and T = 46 °C) under 365 nm irradiation.

CP1 and (2.56 eV) of CP2 were within the range of semiconductors.

To investigate the mechanism, we collected the final photodegradation products. First, after irradiating the IBP solution for 30 min, the intermediate products were extracted with diethyl ether. The solution was concentrated under a stream of nitrogen until the ether had evaporated. The residue is dissolved with the appropriate solvent for GC/MS analysis.

The main photoproducts were analyzed by GC/MS. Besides the ibuprofen, four intermediate products were identified. These byproducts are summarized in Table 2.

The possible photocatalytic mechanism proposed for the degradation of IBP by the coordination polymers is as follows (Scheme 2).

At the beginning, the IBP molecules are adsorbed on the surface of CP and initiate the photo excitation process.

With the increasing catalyst loading, generation of radicals enhanced the degradation process. Degradation was evidenced from the decrease within the severity of the spectral peak rather like the IBP (m/z 205), which was clearly observed with m/z = 207.[49]
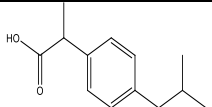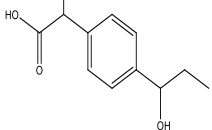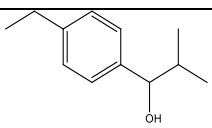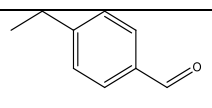
Direct demethylation of IBP at the α position and hydroxylation results in product (1), m/z = 191. Subsequent decarboxylation leads to1-(4-ethyl-phenyl)-2-methyl-propan-1-ol (2) with m/z = 177, previously reported by Lei et al.[50] A C−C scission can cause the cleavage of the isobutyl moiety from photoproduct (2), leading to photoproduct 4-ethylbenzalde-hyde (3), with m/z = 134. The swift reaction of reactive species with 4-ethylbenzaldehyde opens the benzyl rings and ultimately produces CO_2 and H_2O.[51] Further transformation photoproducts could be formed from the attack by reactive species like ●O^{2-},[52] but the above-mentioned intermediates (1, 2, and 3) are the main degradation products, which suggests that hydroxylation is the main pathway.[53−56]

3. CONCLUSIONS

This study addresses the synthesis of two Zn-based semi-conductors belonging to the class of coordination compounds (CPs), with the ultimate aim to enhance the potential of Zn coupled to solar natural light to photocatalyze the degradation of drinking water pollutants. This could be achieved by combining Zn with organic ligands, namely, 4,4′-bipyridine, 8-hydroxyquinoline, or terephthalic acid.

The synthesized CPs decreased the ZnO energy gap value, thanks to their conjugated electronic doublets, whose

Table 2. Main Products Observed by GC–MS (ESI Negative Scan Mode) for the IBP/CP1/H$_2$O$_2$/UV System after 60 min of 365 nm Irradiation

name	molecular	M/S ([M−H]$^-$)	t_r (min)	references
ibuprofen		207	10.71	
hydroxy-ibprofen (1)		209	9.30	49
1-(4-ethyl-phenyl)-2-methyl-propan-1-ol (2)		177	9.15	50
4-ethylbenzaldehyde (3)		134	8.99	51,56

abundance facilitates electron promotion to the conduction band while shifting the transition to longer wavelengths. Synthesis of CP1 involved a bipyridine as an *N*-donor and terephthalic acid as a coligand. In the case of CP2, 8-hydroxyquinoline was used while maintaining terephthalic acid as a coligand.

X-ray powder diffraction showed that CP1 is crystalline, while CP2 required a further recrystallization step. FTIR confirmed the existence of the anticipated chemical bonds. TGA confirmed CPs' stability up to 100 °C. The structural study revealed original structures, and CP1 is fair, while in CP2, the metal was shown to be encapsulated. The experimentally determined energy gaps are 2.69 eV for CP1 and 2.56 eV for CP 2, values that are much lower than those of ZnO (3.37 eV), extending the absorption range to higher wavelengths of the solar light spectrum. High IBP degradation extents were achieved (84% for CP1 and 70.6% for CP2, in a 60 min irradiation time), confirming the photocatalyst's efficiency. The photodegradation reactions exhibited uncommon pseudo-zero-order kinetics. The positive outcomes reached by the current work prompted us to design some more functional crystalline solids, with even higher stability and efficiency, by using positional isomeric bipyridine ligands and other aromatic bicarboxylate ligands as spacers. Efforts on this approach are currently underway in our lab.

4. EXPERIMENTAL METHODS

4.1. Chemical Synthesis. *4.1.1. Synthesis of Coordination Polymer CP1 and CP2 Was Conducted Using the Hydrothermal Method. 4.1.1.1. CP1: {[Zn(II)(BIPY)(Pht)]·H$_2$O}$_n$.* Under continuous stirring, 0.078 g (0.5 mmol) of 4.4′ bipyridine was dissolved in ethanol (5 mL) and slowly added to a solution containing 0.166 g (1 mmol) of terephthalic acid dissolved in a mixture of 7 mL of H$_2$O and 3 mL of ethanol. Then, 0.148 g (0.5 mmol) of Zn(NO$_3$)$_2$·6H$_2$O was subsequently added to the above solution. The
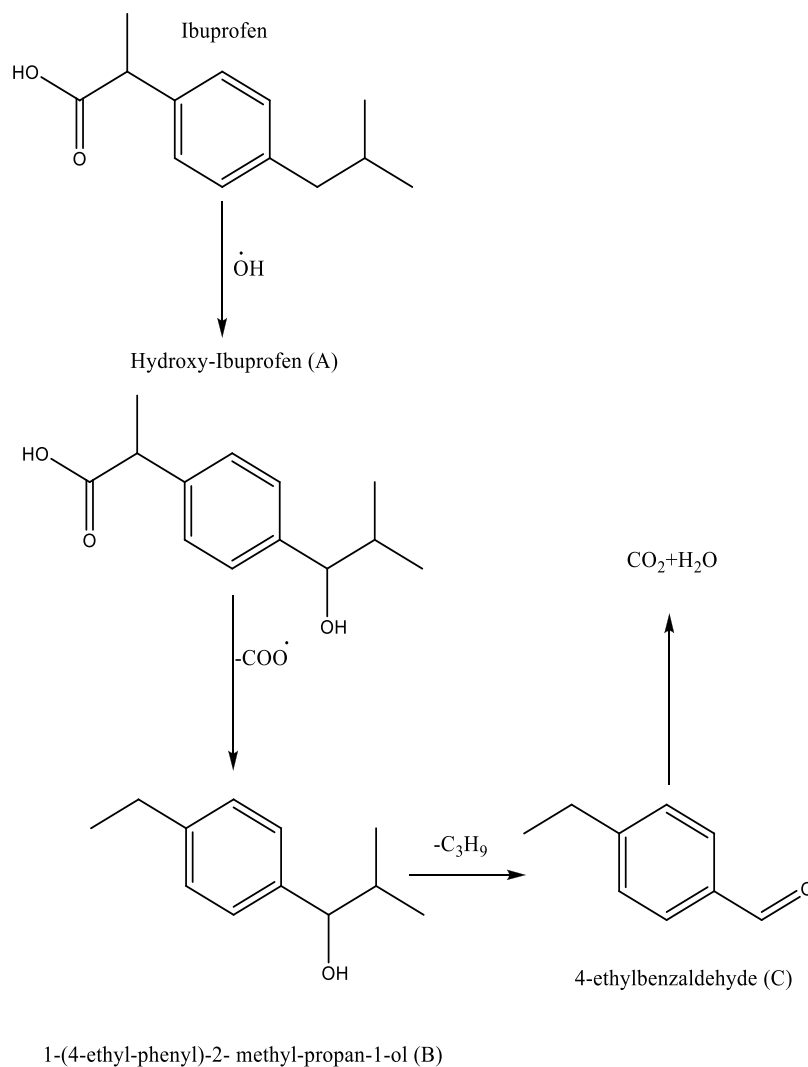
mixture was transferred into a 25 mL sealed Teflon, placed in an autoclave set at 200 °C for 72 h, and then cooled at room temperature. The precipitate was filtered off. The yellow filtrate (pH = 4.28) was allowed to dry slowly at room temperature. Yellow crystals appeared after a few days, evidencing the incorporation of the initial ligand, with a yield of 72%. Experimental and simulated XRD patterns are in good agreement, pointing to a good phase purity (Figure 2a).

4.1.1.2. CP2: {[Zn(II)(HYD)(Pht)]}$_n$. A suspension of Zn(NO$_3$)$_2$·6H$_2$O (30.8 mg, 0.1 m mol), 8-hydroxyquinoline (14.5 mg—0.1 mmol), terephthalic acid (16.8 mg, 0.1 mmol), and NaOH (8 mg, 0.2 mmol) in 10 mL of distilled H$_2$O was introduced in a 25 mL steel Teflon, sealed, and heated at 130 °C for 3 days. After cooling the mixture to ambient temperature at a rate of 5 °C h^{-1}, a red powder was obtained with a yield of 70% (Figure 2a).

4.2. Materials Characterization. The powder structure was characterized by XRD using a PANalytical X-ray diffractometer equipped with CuKα radiation. Infrared spectra were recorded on a Varian 640 FTIR spectrometer in KBr pellets within the range of 500–4000 cm^{-1}. Thermal analysis was run on a Shimadzu thermogravimetric analyzer (TGA) at a heating rate of 10 °C min^{-1} in a nitrogen atmosphere. IR samples were prepared as discs obtained from a 200 mg aliquot of the powder mixture (KBr/CP I = 100:1) desiccated for 30 min. IR spectra were obtained using a Nicolet Magna 550 II FT-IR spectrophotometer within the wavelength range of 4000–400 cm^{-1}. UV/vis absorption spectroscopy was performed with a Hitachi U-3010 spectrophotometer. For the electrochemical study, the cyclic voltammetry curves were acquired with an electronic assembly of a potentiostat/galvanostat Volta Lab PGZ301 assisted by a computer and a measuring cell.

4.3. Photocatalytic Activity. The reactivity of the monodisperse complex was tested by the degradation of ibuprofen in solution. The test was conducted in a Pyrex

Scheme 2. Possible Photocatalytic Mechanism Proposed for the Degradation of IBP by the Coordination Polymers

Ibuprofen

↓ $\dot{O}H$

Hydroxy-Ibuprofen (A)

$CO_2 + H_2O$

↓ -COO·

1-(4-ethyl-phenyl)-2- methyl-propan-1-ol (B)

-C₃H₉ →

4-ethylbenzaldehyde (C)

reactor (diameter: 2 cm; total capacity: 50 mL), with a cooling device, and placed in an elliptical compartment. The reaction mixture was stirred continuously with a magnetic bar. The tests were run at (20 ± 1) °C, in an isothermal reaction system, with the temperature being maintained constant with a water bath. The sample solution was irradiated with a lamp (Philips 15W TL-D), which emits a polychromatic radiation centered at 365 nm. The distance, separating the lamp and the reactor wall, is 10 cm. Solar irradiation tests were carried outdoors, in an open space neighboring the building hosting our laboratory in Constantine, Figure 17.

Figure 17. LSTE laboratory platform sun light in Constantine. Photograph courtesy of Adala Amina.

The sunlight intensity (May 2020) was measured at different time intervals. The mean values of the intensities are gathered in Table 3.

Table 3. Average Values of Sunlight Intensity

day	1	2	3
light intensity (mW cm⁻²)	2.149	2.432	1.542

To work out the adsorption−desorption equilibrium, a 1 g/ L suspension of the coordination polymer was added to100 mL of 5.10^{-5} M ibuprofen. The mixture was maintained in the dark for 30 min, under continuous stirring with a magnetic stirrer. Then, 4 mL was withdrawn at selected time intervals from the reaction mixture and immediately centrifuged to quickly remove the photocatalyst; the supernatant solution was analyzed with a Shimadzu LC-20C high-performance liquid chromatography instrument, equipped with a Supelco HC-C 18 column (5 μm × 4.6 mm). The mobile phase is a 60/40 mixture of acetonitrile and ultrapure water, with a 1.0 mL min⁻¹ flow rate. The detection wavelength was set at 222 nm.

■ APPENDIX A. SUPPLEMENTARY

■ ASSOCIATED CONTENT

ⓈI Supporting Information

■ AUTHOR INFORMATION

Corresponding Author

  Amina Adala − *Department of Chemistry, Mentouri Brothers University, Constantine 25017, Algeria; Laboratory of Sciences and Technologies of Environment, Constantine 25017, Algeria;* ◉ orcid.org/0000-0001-8982-2745; Phone: +123 (0)657665888; Email: adala.amina@umc.edu.dz

Authors

  Nadra Debbache − *Department of Chemistry, Mentouri Brothers University, Constantine 25017, Algeria; Laboratory of Sciences and Technologies of Environment, Constantine 25017, Algeria*

  Tahar Sehili − *Department of Chemistry, Mentouri Brothers University, Constantine 25017, Algeria; Laboratory of Sciences and Technologies of Environment, Constantine 25017, Algeria*

Complete contact information is available at:
https://pubs.acs.org/10.1021/acsomega.1c06049

Notes

The authors declare no competing financial interest.

■ ACKNOWLEDGMENTS

■ REFERENCES

(1) Quici, N.; Morgada, M. E.; Gettar, R. T.; Bolte, M.; Litter, M. I. Photocatalytic degradation of citric acid under different conditions: TiO2 heterogeneous photocatalysis against homogeneous photolytic processes promoted by Fe (III) and H2O2. *Appl. Catal., B* **2007**, *71*, 117−124.

(2) Ou, X.; Quan, X.; Chen, S.; Zhang, F.; Zhao, Y. Photocatalytic reaction by Fe (III)−citrate complex and its effect on the photodegradation of atrazine in aqueous solution. *J. Photochem. Photobiol., A* **2008**, *197*, 382−388.

(3) Nansheng, D.; Feng, W.; Fan, L.; Mei, X. Ferric citrate-induced photodegradation of dyes in aqueous solutions. *Chemosphere* **1998**, *36*, 3101−3112.

(4) Hug, S. J.; Canonica, L.; Wegelin, M.; Gechter, D.; Von Gunten, U. Solar oxidation and removal of arsenic at circumneutral pH in iron containing waters. *Environ. Sci. Technol.* **2001**, *35*, 2114−2121.

(5) Abrahamson, H. B.; Rezvani, A. B.; Brushmiller, J. G. Photochemical and spectroscopic studies of complexes, of iron (III) with citric acid and other carboxylic acids. *Inorg. Chim. Acta* **1994**, *226*, 117−127.

(6) García-Montaño, J.; Pérez-Estrada, L.; Oller, I.; Maldonado, M. I.; Torrades, F.; Peral, J. Pilot plant scale reactive dyes degradation by solar photo-Fenton and biological processes. *J. Photochem. Photobiol., A* **2008**, *195*, 205−214.

(7) Kritikos, D. E.; Xekoukoulotakis, N. P.; Psillakis, E.; Mantzavinos, D. Photocatalytic degradation of reactive black 5 in aqueous solutions: Effect of operating conditions and coupling with ultrasound irradiation. *Water Res.* **2007**, *41*, 2236−2246.

(8) Li, M.; Liu, L.; Zhang, L.; Lv, X.; Ding, J.; Hou, H.; Fan, Y. Novel coordination polymers of Zn (II) and Cd (II) tuned by different aromatic polycarboxylates: synthesis, structures and photocatalytic properties. *CrystEngComm* **2014**, *16*, 6408−6416.

(9) Dai, M.; Su, X. R.; Wang, X.; Wu, B.; Ren, Z. G.; Zhou, X.; Lang, J. P. Three zinc (II) coordination polymers based on tetrakis (4-pyridyl) cyclobutane and naphthalenedicarboxylate linkers: solvothermal syntheses, structures, and photocatalytic properties. *Cryst. Growth Des.* **2014**, *14*, 240−248.

(10) Benhassine, A.; Boulebd, H.; Anak, B.; Bouraiou, A.; Bouacida, S.; Bencharif, M.; Belfaitah, A. Copper (II) and zinc (II) as metal-carboxylate coordination complexes based on (1-methyl-1H-benzo [d] imidazol-2-yl) methanol derivative: Synthesis, crystal structure, spectroscopy, DFT calculations and antioxidant activity. *J. Mol. Struct.* **2018**, *1160*, 406−414.

(11) Xu, L.; Fang, H.; Li, S.; Zhu, J.; Pan, C.; Pan, Y.; Feng, Q. Tailored Hydrothermal Synthesis of Specific Facet-Dominated TiO2 Nanocrystals from Lepidocrocite-Type Layered Titanate Nanosheets: Systematical Investigation and Enhanced Photocatalytic Performance. *Langmuir* **2020**, *36*, 4477−4495.

(12) Zhang, X.; Fan, L.; Fan, W.; Li, B.; Zhao, X. Assembly of a series of d 10 coordination polymers based on W-shaped 1, 3-di (2′, 4′-dicarboxyphenyl) benzene: from syntheses, structural diversity, luminescence, to photocatalytic properties. *CrystEngComm* **2015**, *17*, 6681−6692.

(13) Pettinari, C.; Tăbăcaru, A.; Galli, S. Coordination polymers and metal−organic frameworks based on poly (pyrazole)-containing ligands. *Coord. Chem. Rev.* **2016**, *307*, 1−31.

(14) Zhao, S.; Li, M.; Shi, L. L.; Li, K.; Li, B. L.; Wu, B. Syntheses, structures and photocatalytic properties of three copper (II) coordination polymers. *Inorg. Chem. Commun.* **2016**, *70*, 185−188.

(15) Wang, C. Y.; Wilseck, Z. M.; LaDuca, R. L. 1D+ 1D→ 1D polyrotaxane, 2D+ 2D→ 3D interpenetrated, and 3D self-penetrated divalent metal terephthalate bis (pyridylformyl) piperazine coordination polymers. *Inorg. Chem.* **2011**, *50*, 8997−9003.

(16) (a) Cui, Y.; Yue, Y.; Qian, G.; Chen, B. Luminescent functional metal−organic frameworks. *Chem. Rev.* **2012**, *112*, 1126−1162. (b) Chang, Y. C.; Wang, S. L. From stimuli-responsive polymorphic organic dye crystals to photoluminescent cationic open-framework metal phosphate. *J. Am. Chem. Soc.* **2012**, *134*, 9848−9851.

(17) (a) Yu, Z. T.; Liao, Z. L.; Jiang, Y. S.; Li, G. H.; Chen, J. S. Water-Insoluble Ag−U−Organic Assemblies with Photocatalytic Activity. *Chem. − Eur. J.* **2005**, *11*, 2642−2650. (b) Lin, H.; Maggard, P. A. Synthesis and structures of a new series of silver-vanadate hybrid solids and their optical and photocatalytic properties. *Inorg. Chem.* **2008**, *47*, 8044−8052. (c) Liao, Z. L.; Li, G. D.; Bi, M. H.; Chen, J. S. Preparation, structures, and photocatalytic properties of three new uranyl− organic assembly compounds. *Inorg. Chem.* **2008**, *47*, 4844−4853. (d) Wang, F.; Liu, Z. S.; Yang, H.; Tan, Y. X.; Zhang, J. Hybrid zeolitic imidazolate frameworks with catalytically active TO4 building blocks. *Am. Ethnol.* **2011**, *123*, 470−473. (e) Das, M. C.; Xu, H.; Wang, Z.; Srinivas, G.; Zhou, W.; Yue, Y. F.; Chen, B. A Zn 4 O-containing doubly interpenetrated porous metal−organic framework for photocatalytic decomposition of methyl orange. *Chem. Commun.* **2011**, *47*, 11715−11717.

(18) Behnajady, M. A.; Modirshahla, N.; Shokri, M. Photo-destruction of Acid Orange 7 (AO7) in aqueous solutions by UV/H2O2: influence of operational parameters. *Chemosphere* **2004**, *55*, 129−134.

(19) Qin, J. S.; Zhang, S. R.; Du, D. Y.; Shen, P.; Bao, S. J.; Lan, Y. Q.; Su, Z. M. A microporous anionic metal−organic framework for sensing luminescence of lanthanide (III) ions and selective absorption of dyes by ionic exchange. *Chem. − Eur. J.* **2014**, *20*, 5625−5630.

(20) Wen, X.; Wang, S.; Ding, Y.; Wang, Z. L.; Yang, S. Controlled growth of large-area, uniform, vertically aligned arrays of α-Fe2O3 nanobelts and nanowires. *J. Phys. Chem. B* **2005**, *109*, 215−220.

(21) (a) Pandey, S.; Das, P. P.; Singh, A. K.; Mukherjee, R. Cobalt (ii), nickel (ii) and copper (ii) complexes of a hexadentate pyridine amide ligand. Effect of donor atom (ether vs. thioether) on coordination geometry, spin-state of cobalt and M III−M II redox potential. *Dalton Trans.* **2011**, *40*, 10758−10768. (b) Singh, A. K.; Mukherjee, R. Structure and properties of bivalent nickel and copper complexes with pyrazine-amide-thioether coordination: stabilization of trivalent nickel. *Dalton Trans.* **2005**, *17*, 2886−2891. (c) Benvidi, A.; Kakoolaki, P.; Gorji, A. R.; Mazloum-Ardakani, M.; Zare, H. R.; Vafazadeh, R. Application of Co (II) complex multi-wall carbon nanotube modified carbon paste electrodes for electrocatalytic determination of hydroxylamine. *Anal. Methods* **2013**, *5*, 6649−6655. (d) Allen, C. A. L. *Tolerance of Metal-Organic Frameworks to Functionalization*; Doctoral dissertation, UC San Diego, 2014.

(22) (a) Jing, H. P.; Wang, C. C.; Zhang, Y. W.; Wang, P.; Li, R. Photocatalytic degradation of methylene blue in ZIF-8. *RSC Adv.* **2014**, *4*, 54454−54462. (b) Cui, L. S.; Meng, X. M.; Li, Y. G.; Huang, K. R.; Li, Y. C.; Long, J. Q.; Yao, P. F. Syntheses, structural diversity, and photocatalytic-degradation properties for methylene blue of Co (ii) and Ni (ii) MOFs based on terephthalic acid and different imidazole bridging ligands. *CrystEngComm* **2019**, *21*, 3798−3809.

(23) Zhang, G.; Fu, Y.; Xie, Z.; Zhang, Q. Synthesis and photovoltaic properties of new low bandgap isoindigo-based conjugated polymers. *Macromolecules* **2011**, *44*, 1414−1420.

(24) Cornell, R. M., Schwertmann, U. *The iron oxides: structure, properties, reactions, occurrences and uses*; John Wiley & Sons, 2003.

(25) Jubb, A. M.; Allen, H. C. Vibrational spectroscopic characterization of hematite, maghemite, and magnetite thin films produced by vapor deposition. *ACS Appl. Mater. Interfaces* **2010**, *2*, 2804−2812.

(26) Strathmann, T. J.; Stone, A. T. Reduction of oxamyl and related pesticides by FeII: influence of organic ligands and natural organic matter. *Environ. Sci. Technol.* **2002**, *36*, 5172−5183.

(27) Bordiga, S.; Lamberti, C.; Ricchiardi, G.; Regli, L.; Bonino, F.; Damin, A.; Zecchina, A. Electronic and vibrational properties of a MOF-5 metal−organic framework: ZnO quantum dot behaviour. *Chem. Commun.* **2004**, *20*, 2300−2301.

(28) Mechakra, H.; Sehili, T.; Kribeche, M. A.; Ayachi, A. A.; Rossignol, S.; George, C. Use of natural iron oxide as heterogeneous catalyst in photo-Fenton-like oxidation of chlorophenylurea herbicide in aqueous solution: Reaction monitoring and degradation pathways. *J. Photochem. Photobiol., A* **2016**, *317*, 140−150.

(29) Kribéche, M. E. A.; Mechakra, H.; Sehili, T.; Brosillon, S. Oxidative photodegradation of herbicide fenuron in aqueous solution by natural iron oxide α-Fe2O3, influence of polycarboxylic acids. *Environ. Technol.* **2016**, *37*, 172−182.

(30) Buxton, G. V.; Greenstock, C. L.; Helman, W. P.; Ross, A. B. Critical review of rate constants for reactions of hydrated electrons, hydrogen atoms and hydroxyl radicals (· OH/· O− in aqueous solution). *J. Phys. Chem. Ref. Data* **1988**, *17*, 513−886.

(31) Ding, X.; Zhao, K.; Zhang, L. Enhanced photocatalytic removal of sodium pentachlorophenate with self-doped Bi2WO6 under visible light by generating more superoxide ions. *Environ. Sci. Technol.* **2014**, *48*, 5823−5831.

(32) Wang, H.; Wang, J. Comparative study on electrochemical degradation of 2, 4-dichlorophenol by different Pd/C gas-diffusion cathodes. *Appl. Catal., B* **2009**, *89*, 111−117.

(33) Huang, C. P.; Chu, C. S. Indirect electrochemical oxidation of chlorophenols in dilute aqueous solutions. *J. Environ. Eng.* **2012**, *138*, 375−385.

(34) Lair, A.; Ferronato, C.; Chovelon, J. M.; Herrmann, J. M. Naphthalene degradation in water by heterogeneous photocatalysis: an investigation of the influence of inorganic anions. *J. Photochem. Photobiol., A* **2008**, *193*, 193−203.

(35) Daneshvar, N.; Behnajady, M. A.; Asghar, Y. Z. Photooxidative degradation of 4-nitrophenol (4-NP) in UV/H2O2 process: Influence

of operational parameters and reaction mechanism. *J. Hazard. Mater.* **2007**, *139*, 275−279.

(36) Kochany, J. Effects of carbonates on the aquatic photodegradation rate of bromoxynil (3, 5-dibromo-4-hydroxybenzonttrile) herbicide. *Chemosphere* **1992**, *24*, 1119−1126.

(37) Piscopo, A.; Robert, D.; Weber, J. V. Influence of pH and chloride anion on the photocatalytic degradation of organic compounds: Part I. Effect on the benzamide and para-hydroxybenzoic acid in TiO2 aqueous solution. *Appl. Catal., B* **2001**, *35*, 117−124.

(38) Chen, H. Y.; Zahraa, O.; Bouchy, M. Inhibition of the adsorption and photocatalytic degradation of an organic contaminant in an aqueous suspension of TiO2 by inorganic ions. *J. Photochem. Photobiol., A* **1997**, *108*, 37−44.

(39) Minero, C.; Mariella, G.; Maurino, V.; Vione, D.; Pelizzetti, E. Photocatalytic transformation of organic compounds in the presence of inorganic ions. 2. Competitive reactions of phenol and alcohols on a titanium dioxide− fluoride system. *Langmuir* **2000**, *16*, 8964−8972.

(40) Wardman, P. Reduction potentials of one-electron couples involving free radicals in aqueous solution. *J. Phys. Chem. Ref. Data* **1989**, *18*, 1637−1755.

(41) De Laat, J.; Le, G. T.; Legube, B. A comparative study of the effects of chloride, sulfate and nitrate ions on the rates of decomposition of H2O2 and organic compounds by Fe (II)/H2O2 and Fe (III)/H2O2. *Chemosphere* **2004**, *55*, 715−723.

(42) Le Truong, G.; De Laat, J.; Legube, B. Effects of chloride and sulfate on the rate of oxidation of ferrous ion by H2O2. *Water Res.* **2004**, *38*, 2384−2394.

(43) Hou, Y. L.; Sun, R. W. Y.; Zhou, X. P.; Wang, J. H.; Li, D. A copper (I)/copper (II)−salen coordination polymer as a bimetallic catalyst for three-component Strecker reactions and degradation of organic dyes. *Chem. Commun.* **2014**, *50*, 2295−2297.

(44) Chen, C.; Ma, W.; Zhao, J. Semiconductor-mediated photodegradation of pollutants under visible-light irradiation. *Chem. Soc. Rev.* **2010**, *39*, 4206−4219.

(45) Zhang, H.; Chen, D.; Lv, X.; Wang, Y.; Chang, H.; Li, J. Energy-efficient photodegradation of azo dyes with TiO2 nanoparticles based on photoisomerization and alternate UV− visible light. *Environ. Sci. Technol.* **2010**, *44*, 1107−1111.

(46) López-Muñoz, M. J.; Aguado, J.; Arencibia, A.; Pascual, R. Mercury removal from aqueous solutions of HgCl2 by heterogeneous photocatalysis with TiO2. *Appl. Catal., B* **2011**, *104*, 220−228.

(47) Zhang, H.; Lv, X.; Li, Y.; Wang, Y.; Li, J. P25-graphene composite as a high performance photocatalyst. *ACS Nano* **2010**, *4*, 380−386.

(48) Gordon, T. R.; Cargnello, M.; Paik, T.; Mangolini, F.; Weber, R. T.; Fornasiero, P.; Murray, C. B. Nonaqueous synthesis of TiO2 nanocrystals using TiF4 to engineer morphology, oxygen vacancy concentration, and photocatalytic activity. *J. Am. Chem. Soc.* **2012**, *134*, 6751−6761.

(49) Shanavas, S.; Priyadharsan, A.; Gkanas, E. I.; Acevedo, R.; Anbarasan, P. M. High efficient catalytic degradation of tetracycline and ibuprofen using visible light driven novel Cu/Bi2Ti2O7/rGO nanocomposite: kinetics, intermediates and mechanism. *J. Ind. Eng. Chem.* **2019**, *72*, 512−528.

(50) Lei, Z. D.; Wang, J. J.; Wang, L.; Yang, X. Y.; Xu, G.; Tang, L. Efficient photocatalytic degradation of ibuprofen in aqueous solution using novel visible-light responsive graphene quantum dot/AgVO3 nanoribbons. *J. Hazard. Mater.* **2016**, *312*, 298−306.

(51) Xiao, Z.; Wang, Y.; Huang, Y. C.; Wei, Z.; Dong, C. L.; Ma, J.; Wang, S. Filling the oxygen vacancies in Co 3 O 4 with phosphorus: an ultra-efficient electrocatalyst for overall water splitting. *Energy Environ. Sci.* **2017**, *10*, 2563−2569.

(52) Liu, S. H.; Tang, W. T. Photodecomposition of ibuprofen over g-C3N4/Bi2WO6/rGO heterostructured composites under visible/solar light. *Sci. Total Environ.* **2020**, *731*, No. 139172.

(53) Liu, S.; Zhang, Z.; Liu, Q.; Luo, H.; Zheng, W. Spectrophotometric determination of vitamin B1 in a pharmaceutical formulation using triphenylmethane acid dyes. *J. Pharm. Biomed. Anal.* **2002**, *30*, 685−694.

(54) da Silva, J. C. C.; Teodoro, J. A. R.; Afonso, R. J. D. C. F.; Aquino, S. F.; Augusti, R. Photolysis and photocatalysis of ibuprofen in aqueous medium: characterization of by-products via liquid chromatography coupled to high-resolution mass spectrometry and assessment of their toxicities against Artemia Salina. *J. Mass Spectrom.* **2014**, *49*, 145−153.

(55) Jallouli, N.; Pastrana-Martínez, L. M.; Ribeiro, A. R.; Moreira, N. F.; Faria, J. L.; Hentati, O.; Ksibi, M. Heterogeneous photocatalytic degradation of ibuprofen in ultrapure water, municipal and pharmaceutical industry wastewaters using a TiO2/UV-LED system. *Chem. Eng. J.* **2018**, *334*, 976−984.

(56) Vickers, N. J. Animal communication: when i'm calling you, will you answer too? *Curr. Biol.* **2017**, *27*, R713−R715.